Clusters of superparamagnetic iron oxide nanoparticles encapsulated in a hydrogel: a particle architecture generating a synergistic enhancement of the T2 relaxation

Paquet, Chantal; de Haan, Hendrick W.; Leek, Donald M.; Lin, Hung-Yu; Xiang, Bo; Tian, Ganghong; Kell, Arnold; Simard, Benoit

Publisher's version / Version de l'éditeur:
https://doi.org/10.1021/nn2002272
ACS Nano, 5, 4, pp. 3104-3112, 2011-03-23

Clusters of Superparamagnetic Iron Oxide Nanoparticles Encapsulated in a Hydrogel: A Particle Architecture Generating a Synergistic Enhancement of the T_2 Relaxation

Chantal Paquet,[†,*] Hendrick W. de Haan,[‡] Donald M. Leek,[†] Hung-Yu Lin,[§] Bo Xiang,[§] Ganghong Tian,[§,∥] Arnold Kell,[†] and Benoit Simard[†,*]

[†]Steacie Institute for Molecular Sciences, National Research Council, 100 Sussex Drive, Ottawa, Ontario, Canada, K1A 0R6, [‡]Department of Physics, University of Ottawa, 150 Louis Pasteur, Ottawa, Ontario, Canada, K1N 6N5, [§]Institute for Biodiagnostics, National Research Council Canada, 435 Ellice Avenue, Winnipeg, MB, R3B1Y6, Canada, and [∥]Department of Physiology, University of Manitoba, 745 Bannatyne Avenue, Winnipeg, Manitoba, Canada R3E 0J9.

ABSTRACT Clusters of iron oxide nanoparticles encapsulated in a pH-responsive hydrogel are synthesized and studied for their ability to alter the T_2-relaxivity of protons. Encapsulation of the clusters with the hydrophilic coating is shown to enhance the transverse relaxation rate by up to 85% compared to clusters with no coating. With the use of pH-sensitive hydrogel, difficulties inherent in comparing particle samples are eliminated and a clear increase in relaxivity as the coating swells is demonstrated. Agreement with Monte Carlo simulations indicates that the lower diffusivity of water inside the coating and near the particle surface leads to the enhancement. This demonstration of a surface-active particle structure opens new possibilities in using similar structures for nanoparticle-based diagnostics using magnetic resonance imaging.

KEYWORDS: superparamagnetic iron oxide nanoparticles · transverse relaxation · contrast agent · hydrogel · pH-responsive · particle coating

Superparamagnetic iron oxide nanoparticles (SPIONs) function as T_2 contrast agents in magnetic resonance imaging (MRI) facilitating the monitoring of disease and the detection of injuries or deficiencies particularly in the liver, spleen, lymph nodes, and bone narrow.[1,2] With new developments of more specialized and efficient contrast agents, MRI has evolved into a versatile technique with multiple functions. For instance, SPION-based contrast agents that generate a target-dependent MRI signal have been used for molecular or cellular detection.[1−3] Efficient contrast agents have also been loaded into cells and used to monitor and track cells *in vivo* by MRI.[2,6,7] However, even with the enhancement of contrast agents, MRI suffers from low sensitivity and as a result there is a need to further improve the efficiency of the contrast agents. This endeavor requires a thorough understanding of the features of contrast agents that increase proton relaxation rates and methods of synthesizing particles that yield these features.

A number of theoretical and experimental studies devoted to examining the effect that iron oxide nanoparticles have on the transverse relaxation rate (R_2) of water protons have demonstrated that the magnetization and the size of the SPIONs are key factors influencing the relaxation rate. More specifically, studies have demonstrated an increase in relaxation rates with increasing magnetization. Accordingly, nanoparticles of various compositions possessing high magnetizations have been synthesized, such as Mn- or Zn-doped ferrites, and have been shown to significantly increase the relaxation rate.[4−6] The effect of particle size has been more difficult to assess due to difficulties in determining accurate sizes and size distributions. However, aggregates of SPIONs have been shown to have dramatically higher relaxation rates compared to single SPIONs.[7] Strategies for preparing SPION-based contrast agents by control aggregation have yielded colloids suitable for MRI with diameters of a few tens of nanometers, a high concentration of SPIONs (*i.e.*, high magnetization), and superparamagnetic properties.[1,8,11−16]

The influence of the particle coating on relaxivity remains unclear as various studies report different effects.[6,9−15] One study using PEGylated SPIONS found that the relaxation rate decreased with increasing PEG length, while their simulations

* Address correspondence to chantal.paquet@nrc.ca, benoit.simard@nrc.ca.

Received for review January 19, 2011 and accepted March 23, 2011.

Published online March 23, 2011
10.1021/nn2002272

predicted that the coating causes competing effects that can either increase or decrease relaxivities.[14] Other recent studies reported that relaxivity values are nearly independent of polymer coatings for large magnetic particles (100 nm), while the relaxation rates of smaller particles (10 nm) were dramatically reduced when coated with silica.[18,19] Another report showed that increasing the hydrophilicity of the particle coating leads to enhanced interactions between the protons with the magnetic core thereby increasing the relaxivity.[13] Recently, Monte Carlo simulations illustrated that some of these discrepancies in effects are attributed to differences in particle size (or dephasing mechanism) and coating composition.[11,12]

Herein, we prepare a unique architecture consisting of a core of densely packed SPIONs encapsulated in a pH sensitive hydrogel. We show that this particle architecture possesses three features key to achieving high and responsive T_2 relaxivities. First, the core of densely packed SPIONs generates high relaxivities due to the resulting high magnetic moment of the particles. Second, the hydrogel coating further increases the relaxivities by prolonging the interaction between the water protons and the high magnetic fields near the particle. Third, the pH-responsive hydrogel coating that swells at high pH values (>5.5) and collapses at low pH values (<4) yields pH-dependent relaxivities. Our results clearly demonstrate that particles coated with a hydrogel have dramatically greater relaxivities in comparison to uncoated particles. In addition, by controlling the pH and increasing the swelling of the coating, we show that the relaxivity can be further increased. To elucidate the precise mechanism of this enhancement, we performed Monte Carlo simulations on protons moving through analogous particles. The simulations confirm that the enhancement is due to the hydrogel coating causing a decrease in the diffusion coefficient of water near the surface of the particle, thereby increasing the interaction time between the water protons and the magnetic field generated by the particles. Thus, with this architecture of particle, we shed light on how the diffusion of water within a particle coating governs the proton spin relaxivities and show that a magnetic core encapsulated with a hydrogel coating can significantly increase the transverse relaxation rate.

RESULTS AND DISCUSSION

Clusters with No Coating. The contrast agents are synthesized by first preparing a magnetic core of densely packed SPIONS as described elsewhere.[16] Briefly, SPIONs dispersed in toluene are ultrasonicated with an aqueous solution of sodium dodecyl sulfate (SDS). The resulting emulsion is heated to evaporate the toluene generating clusters of SPIONs stabilized by SDS, as shown in the TEM image of Figure 1. As was

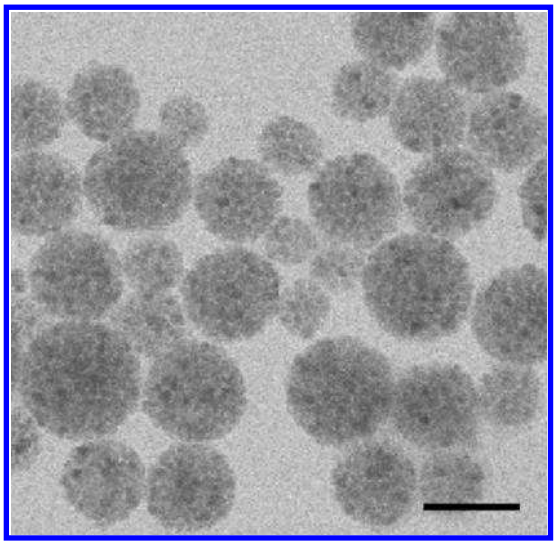

Figure 1. TEM image of cluster of densely packed SPIONs. Scale bar: 100 nm.

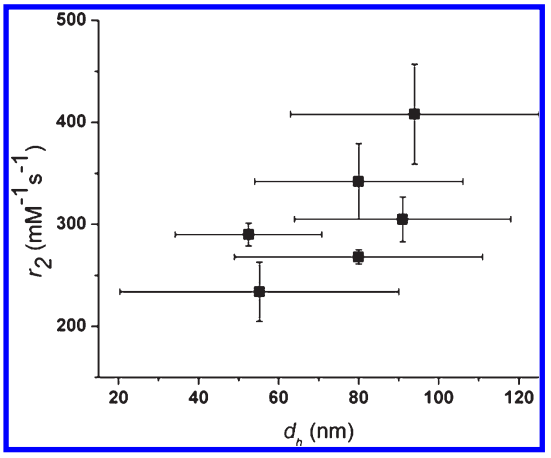

Figure 2. The relaxivity of clusters of various diameters and size distributions. The size distributions of the particles are represented by the bars in the *x*-dimensions.

previously shown, these clusters are monomodal in size and their diameters can easily be controlled by changing the emulsion composition. These clusters were previously shown to consist of ~75% by weight of iron oxide and to have saturation magnetization of ~58 emu/g.[16]

The transverse relaxivity (r_2) of these clusters was first measured as a function of cluster diameter in order to gain an understanding of the size effects on r_2. The relaxivity of clusters with number-averaged hydrodynamic diameters ranging from 53 to 94 nm (see Table S1 in the Supporting Information for the TEM diameters) are shown in Figure 2 with the standard deviation in their diameters represented by the bars in the *x*-dimension. The high relaxivities of these clusters, ranging between 245 and 410 mM^{-1} s^{-1}, can be attributed to their structure: densely packed nanoparticles have high magnetizations.[7,17] Similar to what has been reported using single SPIONs, the relaxivities of

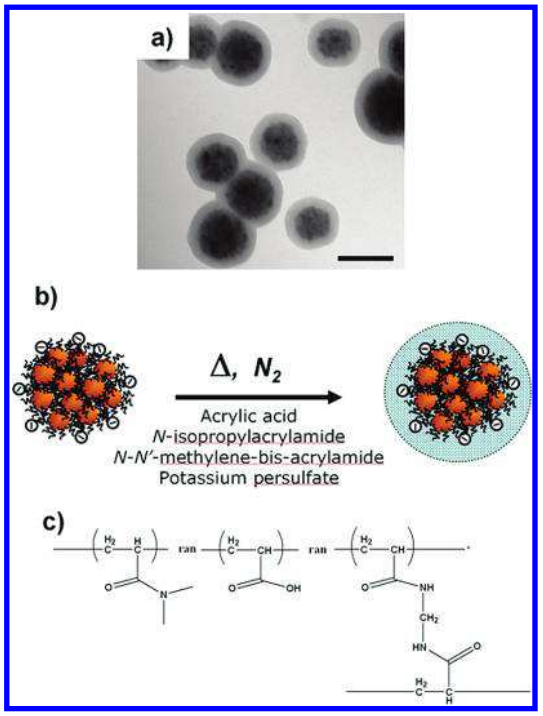

Figure 3. (a) TEM image of clusters encapsulated in a hydrogel. Scale bar: 100 nm. (b) Schematic representation of the precipitation polymerization of the hydrogel unto the surface of the cluster. (c) Structure of the hydrogel polymer.

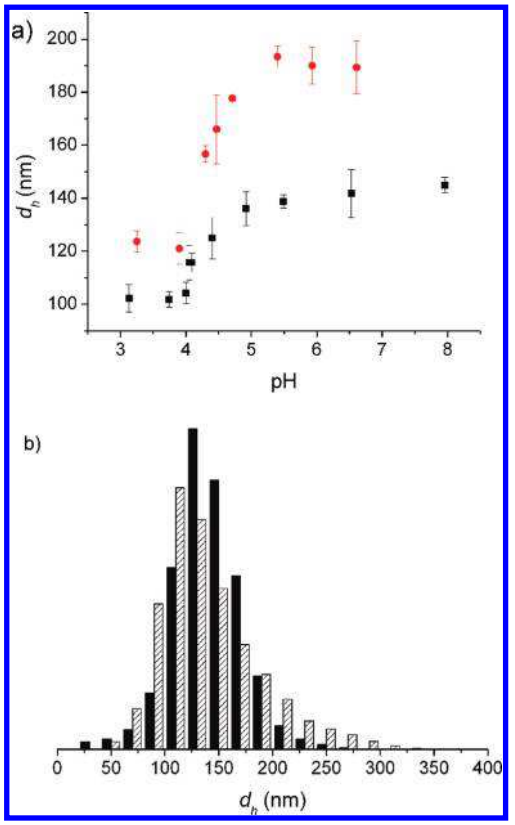

Figure 4. (a) The hydrodynamic diameter of the clusters with a thin (black squares) and with a thick (red circles) hydrogel coating as a function of the pH of the dispersing water. (b) The size distribution of the clusters with a thin shell, before (solid bars) and after (hatched bars) their collapse at pH 3.5 and recovery back to pH 7.

the clusters are also found to increase with increasing diameter.[6] However, the clusters show a poorly defined dependence of relaxivity on the diameter, which can be ascribed to the difficulties obtaining accurate sizes as well as the differences in the size distribution of each batch of particles. These results highlight the challenges in obtaining accurate comparisons of relaxation rates from particles prepared at different times and possessing different size distributions. In what follows, by using a single batch of clusters coated with a pH-responsive polymer, we studied how the hydrogel coatings govern the relaxation rates, thereby eliminating any variability that can arise from the size determination and variations in size distributions.

Hydrogel-Coated Clusters. Using precipitation polymerization concepts, a hydrogel coating composed of 4.5% (molar) acrylic acid, 9.0% (molar) *N,N′*-methylene-bis-acrylamide and 86.5% (molar) *N*-isopropylacrylamide was polymerized around the SPION core. A schematic describing this process, along with the molecular structure of the hydrogel and TEM images of representative particles are shown in Figure 3. The thickness of the hydrogel coating was controlled by changing the ratio of the clusters to monomer added. Using the same batch of clusters, with a hydrodynamic diameter (d_h) of 80 ± 30 nm and a diameter based on TEM (d_{TEM}) of 64 ± 16 nm, we prepared hydrogel-coated clusters with a thin and thick polymer shell. The thickness and pH response of the hydrogel coating was characterized by measuring the hydrodynamic diameters of the particles as a function of pH. Figure 4a shows that the diameters of the hydrogel-coated clusters are small at pH values below 4, increase sharply in the range of 4.3−4.7 and plateau at a large diameter for pH values above 5.5. The changes in sizes follow the deprotonation of acrylic acid with increasing pH. At pH values below 4, the acrylic acid is protonated and as a result is neutral. However, the poly(NIPAM-AA) hydrogel is weakly hydrated due to the hydrophilicity of the NIPAM moieties.[18] As the pH increases, the acrylic acid moieties begin to deprotonate, generating electrostatic repulsion within the polymer network thus causing it to swell with water. A steep increase in the diameter of the particles occurs near the pk_a of acrylic acid between a pH of 4.3 to 4.7. Above a pH of 5.5, the acrylic acid moieties are completely deprotonated and the hydrogel network is fully expanded with water maximizing the distance between the charged acrylic acid groups. A comparison of the size distributions of the particles with a thin shell before and after the particles were collapsed at a pH of 3.5 is found in Figure 4b and reveals that the particles recover without any significant increase in average diameter but with a very slight increase in the size distribution (see the Supporting Information for details on pH recovery).

TABLE 1. The Thickness of the Hydrogel Shell, the Relaxivity, the Increase in the Relaxivity with Respect to the Uncoated Particle, the Fraction of Water in the Hydrogel, and the Diffusion Coefficient of Water within the Hydrogel at pH 4, 4.5, and 7

pH	shell thickness (nm)	r_2 (mM^{-1} s^{-1})	% increase in r_2	% water in hydrogel	diffusion coefficient of water (10^{-9} m^2/s)
			Particle with a Thin Shell		
4.0	10	394	44	42	0.2
4.5	22	420	54	70	1.0
7.0	31	436	60	83	1.4
			Particle with a Thick Shell		
4.0	20	467	71	42	0.2
4.5	42	484	77	70	1.0
7.0	54	505	85	83	1.4

Table 1 summarizes the thicknesses of the coatings of each particle at pH values of 4, 4.5, and 7. Briefly, for the cluster with a thin shell, the coating is 10 nm when weakly hydrated (low pH values) and 31 nm when fully hydrated (high pH values). Similarly, the thickness of the shell on the particles with a thick coating is 20 nm when weakly hydrated and 54 nm when strongly hydrated. To avoid ambiguity in discussing the two particles and their pH-dependent volumes, we will refer to the volume of the hydrogel with the water it carries as the shell volume, whereas the clusters with the two different coating thicknesses will be referred to as the clusters with a thick and thin shell.

The relaxivity of the clusters with no shell and with a thin and thick shell were measured at pH values of 4, 4.5, and 7, representing polymer states in a weakly, moderately, and strongly hydrated state, respectively. For these measurements, the particles were embedded in 1% agarose gel, which prevented the magnetic particles from aggregating in the applied magnetic field used during the relaxivity measurements. As a reference point, the relaxivity value of clinically used Feridex was measured as 159 mM^{-1} s^{-1}, while the relaxivity of the clusters with no shell was measured as 273 mM^{-1} s^{-1}. The relaxivities of the clusters with a thin shell reveal a pH dependence with relaxivities of 394, 420, and 436 mM^{-1} s^{-1} at pH 4, pH 4.5, and pH 7, respectively. The clusters with a thick shell demonstrate generally greater relaxivity values but also a weaker pH dependence. At pH 4, pH 4.5, and pH 7, the relaxivities of the clusters with a thick shell are 467, 484, and 505 mM^{-1} s^{-1}, respectively. These values, found in Table 1, demonstrate that the relaxivities of the hydrogel-coated clusters are all significantly greater than the clusters with no shell, with the relaxivities increasing from 44 to 85% from the bare particle value depending on the thickness and degree of swelling of the coating. We note that relaxivity measurements performed on a control sample consisting of blank hydrogel colloids (no SPIONs) did not generate any changes in the relaxation rate of protons at pH 4–7, ruling out the possibility that the hydrogel itself increases the relaxation rate. In addition, measurements made on a mixture of clusters with no shell and hydrogel colloids yielded relaxivities of 277 mM^{-1} s^{-1}, a value commensurate with the relaxivities of clusters with no shell. Therefore, the particle architecture of a magnetic core encapsulated by hydrogel governs the relaxation rate. Further, the degree of enhancement is dependent on the level of hydration of the polymer and its thickness.

Proton Dephasing Mechanisms. The relaxivities of these particles illustrate that hydrophilic coatings have a dramatic impact on the relaxivities. To elucidate the role of the coating, the mechanism of transverse relaxation of water protons in the presence of magnetic particles must be considered.[19] The transverse relaxation is the decay of coherently precessing spins to a state where the proton magnetic spins are precessing out of phase. The addition of magnetic particles to the system introduces local perturbations in the magnetic field, thereby influencing the precessing frequencies of the individual protons. The rate at which protons dephase depends on the balance between the magnetic field perturbation generated by the particle and the diffusivity of the proton. Three dephasing mechanisms have been defined and classified on the basis of particle size at constant volume fraction of particles. For small particles, protons dephase according to the motional averaging regime (MAR). In this regime, the distance traveled by a proton by diffusion is much larger than the average distance between particles and as a result, protons readily diffuse to a different magnetic environment before becoming fully dephased. As protons are not fully dephased in a single encounter with a particle, refocusing will occur when protons diffuse to a magnetic environment of opposite polarity, thereby retarding the overall relaxation rate. Relaxation rates in MAR, therefore, decrease with decreasing particle sizes due to the greater frequency of diffusion-induced refocusing of protons at smaller sizes than at larger particle sizes. Above a critical particle size, the protons spend a sufficient amount of time near one particle to be fully dephased in a single encounter with a particle. However, the proton must diffuse to within a relatively small distance of a

particle to experience this full dephasing event. Therefore, a proton can be described as diffusing outside of this "full dephasing zone" with minimal dephasing and then experiencing rapid and full dephasing on diffusing into this zone. This dephasing mechanism was introduced by Brooks[20] as the visit-limited regime (VLR) and was recently reexamined by de Haan[11] where the details of this discrete dephasing process were explored. At large particle sizes, the distance between particles is much larger than the distance traveled by the proton due to diffusion. Each proton thus experiences an almost constant magnetic environment and dephasing occurs as an approximately continuous process. As the protons are effectively fixed in place, this regime is named the static dephasing regime (SDR).

For particles coated with a material that is impermeable to water, the relaxation rates are lowered in MAR and VLR because the coating obstructs protons from accessing the dephasing zones near the particles surface.[11,15] In contrast, particle coatings will have little to no effect on the relaxation rates in SDR, since, regardless of their proximity to the particle, protons experience an effectively constant magnetic environment.[10,11] The case for hydrophilic coatings, however, is dramatically different from coatings that are impermeable to water since these coatings will alter the proton trajectories in two ways. First, hydrophilic coatings such as hydrogels can decrease the self-diffusion coefficient of water.[21−23] Therefore, the coating slows down water molecules inside of it and holds them in regions near the particle for longer periods than for bare particles. However, this increased residence time also implies a slower exchange of water molecules between the inside and outside of the coating. These two effects affect the dephasing of protons differently depending on the dephasing mechanism.[12] In MAR, protons are not fully dephased in a single encounter when a particle has no coating. By holding water molecules near the particle for longer times, the coating increases the dephasing per encounter and thus reduces diffusion-controlled refocusing. Consequently, the relaxation rate at small particle sizes is greatly enhanced by the introduction of a coating. In VLR, the picture is quite different: even for bare particles, protons can be fully dephased in a single encounter. As a result of the decreased exchange across the coating surface, introduction of a coating around the particles reduces access to the full dephasing zone. Thus, at intermediate particle sizes, a hydrophilic coating actually lowers the relaxation rate. Finally, in SDR, the protons are effectively stationary to begin with. Adding a coating which slows them down even further has no effect, and the relaxation rate is unaffected by a coating. These various effects have been outlined in detail in a previous study by de Haan *et al.*[12]

Given their measured magnetization and size, the particles under study in this work are predicted to dephase according to the MAR and VLR mechanisms. However, several experimental details suggest that the effective particle size and magnetizations are significantly smaller. First, the synthesis of the particle can introduce nonmagnetic material in the core of the particle (*e.g.*, SDS). Further, as can be observed from the difference in the TEM and the hydrodynamic diameter of the particles, a significant hydration layer exists. This layer of water is effectively stationary with respect to the particle thus giving rise to an exclusion layer around the particle. As has been shown, the inclusion of an exclusion layer around a particle reduces its effective size thus reducing the relaxivity in both MAR and VLR.[10,12,14] Finally, for particles dephasing in MAR or VLR, the polydispersity of the sample is likely to be an important factor. Recall that in MAR, the relaxation rate decreases rapidly with decreasing particle size while above MAR, the rate is relatively independent of particle size. Hence, for a distribution of particle sizes around the transition from MAR to VLR, the small particle sizes will have a larger impact and disproportionally reduce the overall relaxation rate. As will be demonstrated, the net effect of these factors is that the particles under study lie in the MAR regime and a hydrophilic coating enhances the relaxivity.

Diffusion Coefficient of Water in the Hydrogel Coatings. To characterize the hydrogel coatings, we estimated the hydrogel volume fraction and the associated diffusion coefficients of water at various pH values. The volume fraction of hydrogel at various pH values was first determined by using data previously reported on colloids of the same composition.[18] For this calculation, the TEM diameter was used to calculate the volume of the colloid in a dehydrated state while the hydrodynamic diameters were used to calculate the water content at various pH values (here the hydration layer at the colloid surface is assumed to be negligible in comparison to the size of the colloid). These calculations yielded water contents in the hydrogel shell of approximately 83, 70, and 42% at pH 7, 4.5, and 4, respectively. Next, using NMR, we measured an *effective* diffusion coefficient of water, D_{H_2O} (population average of free, intermediate and bound water), in hydrogel colloids containing no SPIONs (see Supporting Information). The NMR results show that the diffusion coefficient of water progressively decreases as the hydrogel fraction increases (*i.e.*, D_{H_2O} decreases as the coating shrinks). Table 1 summarizes the estimated fraction of water in the hydrogel at each pH and the corresponding diffusion coefficient of water within the gel. The data shows that D_{H_2O} within the shell drops from a bulk water value of 2.5×10^{-9} m^2/s to 1.4×10^{-9}, 1.0×10^{-9}, and 0.2×10^{-9} m^2/s in the presence of a hydrogel at pHs 7, 4.5, and 4, respectively.

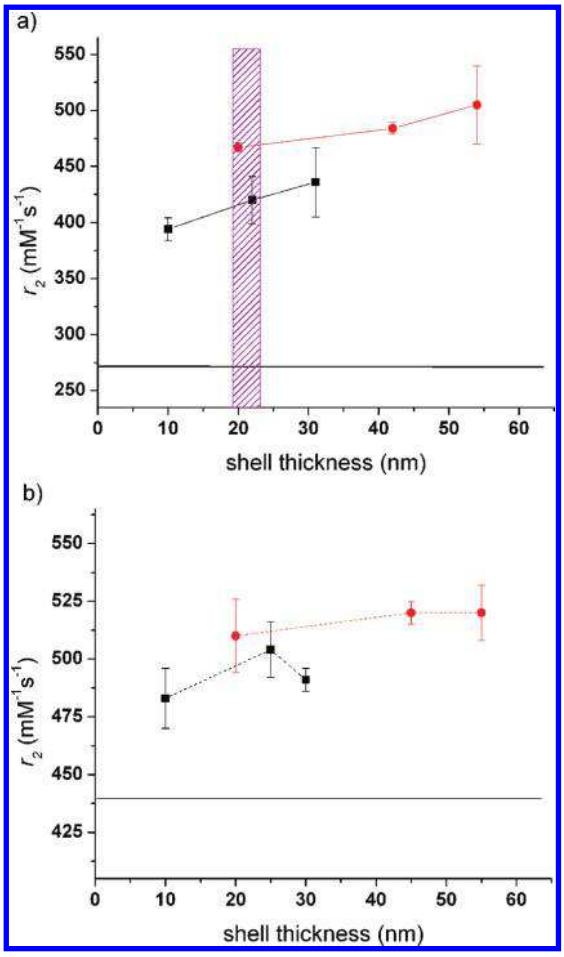

Figure 5. (a) Experimentally measured and (b) simulated dependence of relaxivity of the clusters on the thickness of the hydrogel coating. The horizontal line indicates the relaxivity of the clusters with no shell.

We have plotted the relaxivities as a function of the thickness of the hydrogel shell, as shown in Figure 5a. The two data sets represent the clusters with a thin and thick shell, while the horizontal line indicates the relaxivity of the clusters without a shell. This plot highlights the gain of up to 85% in the relaxivity that was achieved by encapsulating the magnetic cores in a hydrogel shell. Two other effects of the hydrogel coating on relaxivity can be observed. First by comparing the relaxivity of the particles from each data set at their smallest thicknesses (*i.e.*, representing the shells at pH < 4), it is possible to compare the coatings with the same hydration level and as a result, the same D_{H_2O}. The data show that the thicker the hydrogel coating, the higher the relaxivity. Second, the role of D_{H_2O} in the hydrogel can be observed by comparing two data points from each data set that have similar shell thicknesses. As an example, the two data points, highlighted by the hatched rectangle in Figure 5a, have similar shell thicknesses but the cluster with the thick shell (red circle) is weakly hydrated (pH < 4), and as a result the water has a lower D_{H_2O} than the water in the cluster with the thin shell (black square) that is moderately hydrated (pH 4.5). The relaxivity of the former is significantly greater than the latter indicating that the lower the D_{H_2O} in the hydrogel, the greater the enhancement in relaxivity by the hydrogel coating. Interestingly, when the pH is varied, the D_{H_2O} and the thickness of the shell cause opposing changes in the relaxivities. That is, when the pH increases, the volume of the shell increases thereby increasing the volume of the water held by the hydrogel, but the diffusion coefficient of water within the hydrogel increases. The net result reveals that the thickness of the shell dominates: as the pH increases the relaxivity increases. This pH-dependent behavior is weaker for the clusters with a thick shell, appearing to reach an upper limit in the relaxivity of 505 mM^{-1} s^{-1}.

Monte Carlo Simulations. To gain insight into the physical mechanisms behind these results, Monte Carlo simulations of protons diffusing among magnetic particles were performed. Details of the general simulation procedure can be found in previous manuscripts as well in the Methods section.[24−28] In particular, the hydrophilic coating was implemented by a methodology recently developed by de Haan *et al.*[12] In modeling the particles, the diameter of the core was set to 40 nm. To account for the hydrodynamic radius and other effects, a 40 nm thick exclusion layer is included around the core to yield a net particle size of 80 nm in agreement with the experimentally determined hydrodynamic diameter. The smaller size of the magnetic core and the thicker exclusion layer used in the simulation in comparison to the experimental value was chosen to account for several effects not modeled in the simulations. That is, as discussed earlier, the introduction of nonmagnetic material during synthesis, the exclusion layer (*i.e.*, hydration layer) and the effects due to polydispersity suggest that the TEM sizes and previous magnetization measurements are overestimates in the context of proton dephasing. Finally, the coatings are accounted for by encapsulating the particles by a hydrophilic coating with a thickness and diffusion coefficient given by experimentally determined values found in Table 1.

Results from the simulations are included in Figure 5b. Examining Figure 5b, there is good overall agreement in form between the experimental and simulation results. In both experiment and simulation, a coating significantly enhances the relaxivity compared to the bare particles and this enhancement generally grows with increasing layer thickness. However, there are deviations when comparing numbers: simulations consistently yield a higher relaxation rate than experiments. This discrepancy has been observed often in the literature.[8−10,29] Recent work by Chen *et al.*[10] indicates that varying interactions at the interface between the coating and the bulk may play a role. Consequently, more elaborate modeling of the coating may serve to reduce the discrepancy. For example,

changes in the hydration layer that occur after the clusters are coated with a hydrogel are not accounted for in the simulations and may explain the discrepancy between the experimentally determined enhancement of the coating (up to 85%) and the simulated enhancement (18%). Imposing a gradient in the diffusion coefficient such that water nearer to the particle is slowed down to a greater degree could also help bring the results in closer agreement. In spite of these differences, the overall agreement in Figure 5b is sufficient to verify the physical picture leading to the enhanced relaxation rate: water in the coating is held near the particle longer, protons are more dephased per encounter, and the resulting reduced refocusing yields a higher relaxivity. Further, the enhancement generally increases with increasing coating thickness. As discussed earlier, with increasing pH, the coating swells but the diffusion coefficient of water in the coating increases toward the bulk value; these trends have opposing effects on the relaxivity. In agreement with experiments, the increased thickness is the dominant factor for the coatings studied here and the relaxivity generally increases as the coating swells.

CONCLUSION

We prepared and characterized a novel architecture for a MRI contrast agent that builds upon the synergistic effect of clusters of SPIONs and hydrogel coatings. The encapsulation of magnetic particles with a hydrogel significantly enhances the transverse relaxation rates by lowering the diffusion coefficient of water near the particles. The hydrogel coating thus allows water protons to interact longer with the strong magnetic field at the surface of the particle than if a coating was not present. As a result, increased image contrast in an MRI measurement can be achieved by the encapsulation of magnetic particles with a hydrophilic coating of appropriate thickness and density. Further, the diffusivity of the water in the coating and the thickness of the coating can be modulated by the pH of the solution yielding pH-dependent relaxivities. The surface-active property of these particles has important applications in nanoparticle-based diagnostics using MRI. For instance, such particles may be used to detect cancer cells which have more acidic cytosols. Furthermore, particles with coatings that have the ability to induce changes in the diffusivity of water upon binding with target molecules may be envisioned for use in nanoparticles-based diagnostic.[30−32] Also, it may be possible to detect large biomolecules or cells from the changes in the diffusivity of water they induced upon binding with SPION particles. As supported by Monte Carlo simulations, these applications could be realized using smaller clusters with carefully tuned coatings.

METHODS

Materials. ACS grade sodium dodecyl sulfate, acrylic acid, *N,N′*-methylene-bis-acrylamide, *N*-isopropylacrylamide and potassium persulfate were purchased from Sigma-Aldrich. Superparamagnetic iron oxide nanoparticles (SPM NPs) coated with fatty acids were purchased from Ferrotec. The Ferrotec SPIONs were analyzed by image analysis of transmission electron microscopy (TEM) images and found to have a diameter of 9.1 ± 2.7 nm. Water filtered through a Millipore filtration system was used for all syntheses and experiments. Aqueous solutions of various pH values were prepared by adding HCl or NaOH to water and making dilutions to the water in order to reach the desired pH.

Preparation of Clusters. The SPIONs were dispersed in toluene at a concentration of 0.1−0.4 g/mL, depending on the desired size of the cluster. Using a Branson Sonifier 250 at a duty cycle of 50% for 180 s, 1.2 mL of the SPIONs/toluene mixture was sheared in 0.8 mL of a 100 mM SDS aqueous solution. The emulsions were heated at 90 °C for 2 h and water was added intermittently to maintain a constant volume. The clusters were purified and size fractionated with magnetic separation and redispersion in 10 mM SDS solution.

Preparation of Hydrogel-Coated Clusters. Clusters were prepared as described above using a SPION concentration of 0.1 g/mL in toluene. The final solid content of the clusters was 8.2 mg/mL. To prepare clusters with a thin shell, 16.4 mg of the clusters were diluted with 40 mL of 4 mM SDS solution, in a three-neck flask with nitrogen inlet and temperature probe and condenser connected to the necks. The dispersion of clusters was heated to 80 °C under nitrogen to prevent oxygen from quenching the radical initiator. When the temperature reached 45 °C, 2 mg of potassium persulfate was added. A solution containing 10 mL of water, 5 μL of acrylic acid, 10 mg of *N,N′*-methylene-bis-acrylamide, and 95 mg of *N*-isopropylacrylamide was injected to the dispersion once the temperature reached 80 °C. The dispersion was left to react for 3 h. The clusters with a thick shell were prepared in a similar manner by increasing the ratio of monomer to cluster. Thus, 4.9 mg of the clusters dispersion was used and a monomer solution containing, 10 μL of acrylic acid, 144 mg of *N*-isopropylacrylamide and 16 mg of *N,N′*-methylene-bis-acrylamide. The polymer-coated clusters were purified by centrifugation and redispersion in water as well as by magnetic separation.

Preparation of Hydrogel Colloids. In a 500 mL round-bottom, three-neck flask, with a nitrogen inlet, temperature probe and condenser attached, 200 mL of water and 60 mg of potassium persulfate was stirred and heated to 80 °C under nitrogen. A monomer mixture consisting of 0.54 g of *N,N′*-methylene-bis-acrylamide, 5.19 g of *N*-isopropylacrylamide, and 0.27 g of acrylic acid was then added. The monomers were left to react for 4 h. The colloids were purified by centrifugation and dialysis.

Instrumentation. TEM imaging was performed on an Hitachi HD-2000 and H7000. Cluster diameters and size distributions (*i.e.*, standard deviation of the mean diameter) were determined by analyzing at minimum 100 particles of the TEM images using ImageTool software. The hydrodynamic diameter of the particles was measured using a Nanosight LM10. Nanosight LM10 is a nanoparticle tracking analysis system that extracts the hydrodynamic diameter by tracking the Brownian motion of particles on a particle-by-particle basis thereby yielding a number average d_h. A minimum of 100 particles trackings were used to obtained the d_h. The concentration of iron in the particle samples was determined using ICP AES. Pretreatment of these samples involved digesting the nanoparticles in a mixture of HCl and HNO_3 (1:1).

MRI Relaxivity Measurements. Samples were prepared by diluting particles in 0.1% agarose at concentrations ranging from 0.182 to 0.364 mM Fe. The addition of agarose was used for the relaxivity measurements to avoid particle aggregation in the applied magnetic field. A commercial MR contrast agent (Feridex, Bayer, USA) was used as a control. MRI experiments were performed on a 3.0 T MRI scanner (Trio, Siemens Healthcare, Erlangen, Germany). Images were acquired using a head phased-array coil and a spin−echo pulse sequence with an inversion−recovery pulse. A repeated T1-weighted sequence was performed using a constant echo time (TE) of 7 ms and various repetition times (TRs) ranging from 300 to 3200 ms with a TR increment of 200 ms. T1 relaxation times were obtained by a nonlinear least-squares estimation from the multiple T1-weighted MR scans. A T_2-weighted inversion−recovery spin−echo sequence was performed to characterize the T_2 relaxation. T_2 relaxation was calculated using six measurements acquired with a constant TR of 2200 ms and varying TEs of 7, 17, 27, 40, 80, and 100 ms. The relaxivities were calculated at three different cluster concentrations as $r_2 = 1/(T_2 - T_{2background})$[Fe], where $T_{2background}$ is the relaxation time of water in the absence of the SPION particles and [Fe] is the concentration of iron (mmol) of the acid digested particles.

NMR Diffusion Measurements. Diffusion measurements were performed using a Bruker AV-III 400 high resolution NMR spectrometer equipped with a 5 mm broadband z-gradient probe capable of producing gradient strengths of 5.35 g/mm. The hydrogel was transferred to a 5 mm NMR tube for analysis. The standard Bruker version of the LED-BPP pulse sequence was used for diffusion measurements with diffusion times of 60−100 ms depending on the sample. The Bruker *Topspin* software was used for analysis of the diffusion data.[33]

Monte Carlo Simulations. For each data point, four independent system setups are simulated by the following procedure. One hundred particles are placed randomly within a cubic box with a length defined by

$$L = N^{1/3} l = \left(\frac{\frac{4}{3}\pi N}{f}\right)^{1/3} R$$

where $N = 100$ is the number of particles, $f = 3.14 \times 10^{-6}$ is the volume fraction, and $R = 20$ nm is the radius of the magnetic core. Particles are not allowed to overlap at the setup. Next, a proton is placed at a random location within the system. The trajectory of the proton is evolved in time steps of $\Delta t = 1$ ns. At each time step the proton jumps a distance

$$dr = \sqrt{6D\Delta t}$$

in a random direction (D is the diffusion coefficient of water). Jumps that would land the proton within the particle core or the exclusion layer around the core are rejected. Periodic boundary conditions are used to replicate the system in x, y, z to reduce artifacts at the system edges and to keep the proton in the central cell.

The coating is implemented using a methodology recently introduced by de Haan *et al.*[12] For jumps outside of the coating, D is taken to be 2.5×10^{-9} m^2/s. For jumps inside the coating, D is defined by the experimentally determined value. In the event of a jump across the coating surface, the length of the jump inside and outside of the coating is scaled to achieve a proper mix of the two mediums. For jumps from out to in, the portion of the jump inside the coating is reduced to account for the lower D; for jumps from in to out, the portion of the jump in the bulk is increased to account for larger jumps outside of the coating. To preserve the correct proton density, a transition probability is imposed at the coating surface. Jumps from the inside of the coating to outside are always successful. Jumps from outside to inside are accepted with a probability determined from the square root of the ratio of the diffusion coefficients.

At each time step, the net magnetic field from nearby particles at the location of the proton is calculated from

$$\mathbf{B} = \sum_i^{N_p} \frac{\mu_0 \mathbf{M}}{3}\left(\frac{R}{r_i}\right)^3 (3\cos^2(\theta_i) - 1)$$

where N_p is the number of particles considered, $\mu_0 = 4\pi \times 10^{-7}$ H/m is the permeability of free space, $\mathbf{M} = 2.58 \times 10^5$ T/m^3 is the magnetization, r_i is the center to center distance from the ith particle to the proton, and θ_i is the angle between the z axis at the ith particle and the position of the proton. Because of the rapid decline of the magnitude of the magnetic field with increasing distance, only particles with a distance l are considered in this calculation.[11] l is defined to be the length of the volume occupied per particle for an ordered arrangement:

$$l = \left(\frac{V}{N}\right)^{1/3} = \left(\frac{v}{f}\right)^{1/3} = \left(\frac{\frac{4}{3}\pi}{f}\right)^{1/3} R$$

From the net magnetic field, the change of the phase $\Delta\phi$ is approximated at each time step by

$$\Delta\phi = \gamma \mathbf{B} \Delta t$$

where $\gamma = 2.67 \times 10^8$ is the gyromagnetic ratio for water protons.

The above steps are repeated for $N_{p^+} = 2000$ protons per system setup with trajectories of 0.05 ms generated for each proton. From the phase trajectories, the signal corresponding to the correlation among the protons spins is generated from

$$S(t) = \frac{1}{N_{p^+}} \sum_i^{N_{p^+}} \cos(\phi_i(t))$$

The characteristic relaxation rate is obtained by fitting the resulting curve with an exponential decay over the first 0.01 ms. The value of each data point represents the mean of the four rates with the error being the standard deviation of the mean among the four measurements.

Acknowledgment. This work is partially supported by the Canadian Institutes of Health Research. We thank I. Gourevich for performing TEM and N. de Silva for analysis by ICP AES.

Supporting Information Available: Additional details on the magnetization of the nanoparticles and clusters of nanoparticles, particle size analysis, the relaxation rates, and the diffusion coefficient of water in the hydrogels and calculations on converting Fe molarity to volume fraction of clusters. This material is available free of charge *via* the Internet at http://pubs.acs.org.

REFERENCES AND NOTES

1. Weissleder, R.; Kelly, K.; Sun, E. Y.; Shtatland, T.; Josephson, L. Cell-Specific Targeting of Nanoparticles by Multivalent Attachment of Small Molecules. *Nat. Biotechnol.* **2005,** *23*, 1418–1423.
2. Tsourkas, A.; Hofstetter, O.; Hofstetter, H.; Weissleder, R.; Josephson, L. Magnetic Relaxation Switch Immunosensors Detect Enantiomeric Impurities. *Angew. Chem., Int. Ed.* **2004,** *43*, 2395–2399.
3. Kaittanis, C.; Santra, S.; Perez, J. M. Role of Nanoparticle Valency in the Nondestructive Magnetic-Relaxation-Mediated Detection and Magnetic Isolation of Cells in Complex Media. *J. Am. Chem. Soc.* **2009,** *131*, 12780–12791.
4. Jang, J. T.; Nah, H.; Lee, J. H.; Moon, S. H.; Kim, M. G.; Cheon, J. Critical Enhancements of MRI Contrast and Hyperthermic Effects by Dopant-Controlled Magnetic Nanoparticles. *Angew. Chem., Int. Ed.* **2009,** *48*, 1234–1238.
5. Lee, J. H.; Huh, Y. M.; Jun, Y. W.; Seo, J. W.; Jang, J. T.; Song, H. T.; Kim, S.; Cho, E. J.; Yoon, H. G.; Suh, J. S.; *et al.* Artificially Engineered Magnetic Nanoparticles for Ultrasensitive Molecular Imaging. *Nat. Med.* **2007,** *13*, 95–99.
6. Tromsdorf, U. I.; Bigall, N. C.; Kaul, M. G.; Bruns, O. T.; Nikolic, M. S.; Mollwitz, B.; Sperling, R. A.; Reimer, R.; Hohenberg, H.; Parak, W. J.; *et al.* Size and Surface Effects on the MRI Relaxivity of Manganese Ferrite Nanoparticle Contrast Agents. *Nano Lett.* **2007,** *7*, 2422–2427.
7. Ai, H.; Flask, C.; Weinberg, B.; Shuai, X.; Pagel, M. D.; Farrell, D.; Duerk, J.; Gao, J. Magnetite-Loaded Polymeric Micelles

as Ultrasensitive Magnetic-Resonance Probes. *Adv. Mater.* **2005,** *17*, 1949–1952.
8. Qiu, P.; Jensen, C.; Charity, N.; Towner, R.; Mao, C. Oil Phase Evaporation-Induced Self-Assembly of Hydrophobic Nanoparticles into Spherical Clusters with Controlled Surface Chemistry in an Oil-in-Water Dispersion and Comparison of Behaviors of Individual and Clustered Iron Oxide Nanoparticles. *J. Am. Chem. Soc.* **2010,** *132*, 17724–17732.
9. Chen, D. X.; Sun, N.; Gu, H. C. Size Analysis of Carboxydextran Coated Superparamagnetic Iron Oxide Particles Used as Contrast Agents of Magnetic Resonance Imaging. *J. Appl. Phys.* **2009,** *106*, 063906.
10. Chen, D. X.; Sun, N.; Huang, Z. J.; Cheng, C. M.; Xu, H.; Gu, H. C. Experimental Study on T2 Relaxation Time of Protons in Water Suspensions of Iron-Oxide Nanoparticles: Effects of Polymer Coating Thickness and Over-Low 1/T2. *J. Magn. Magn. Mater.* **2010,** *322*, 548–556.
11. de Haan, H. W. Mechanisms of Proton Spin Dephasing in a System of Magnetic Particles. *Magn. Reson. Med.* **2011**, accepted.
12. de Haan, H. W.; Paquet, C. Enhancement and Degradation of the R_2* Relaxation Rate Resulting from the Encapsulation of Magnetic Particles with Hydrophilic Coatings. *Magn. Reson. Med.* **2011**in press.
13. Duan, H.; Kuang, M.; Wang, X.; Wang, Y. A.; Mao, H.; Nie, S. Reexamining the Effects of Particle Size and Surface Chemistry on the Magnetic Properties of Iron Oxide Nanocrystals: New Insights into Spin Disorder and Proton Relaxivity. *J. Phys. Chem. C* **2008,** *112*, 8127–8131.
14. LaConte, L. E. W.; Nitin, N.; Zurkiya, O.; Caruntu, D.; O'Connor, C. J.; Hu, X.; Bao, G. Coating Thickness of Magnetic Iron Oxide Nanoparticles Affects R_2 Relaxivity. *J. Magn. Reson. Imaging* **2007,** *26*, 1634–1641.
15. Pinho, S. L. C.; Pereira, G. A.; Voisin, P.; Kassem, J.; Bouchaud, V.; Etienne, L.; Peters, J. A.; Carlos, L.; Mornet, S.; Geraldes, C. F. G. C. H.; *et al*. Fine Tuning of the Relaxometry of γ-Fe_2O_3@SiO_2 Nanoparticles by Tweaking the Silica Coating Thickness. *ACS Nano* **2010,** *4*, 5339–5349.
16. Paquet, C.; Pagé, L.; Kell, A.; Simard, B. Nanobeads Highly Loaded with Superparamagnetic Nanoparticles Prepared by Emulsification and Seeded-Emulsion Polymerization. *Langmuir* **2010,** *26*, 5388–5396.
17. Larsen, B. A.; Haag, M. A.; Serkova, N. J.; Shroyer, K. R.; Stoldt, C. R. Controlled Aggregation of Superparamagnetic Iron Oxide Nanoparticles for the Development of Molecular Magnetic Resonance Imaging Probes. *Nanotechnology* **2008,** *19*, 265102.
18. Snowden, M. J.; Chowdhry, B. Z.; Vincent, B.; Morris, G. E. Colloidal Copolymer Microgels of *N*-Isopropylacrylamide and Acrylic Acid: pH, Ionic Strength and Temperature Effects. *J. Chem. Soc., Faraday Trans.* **1996,** *92*, 5013–5016.
19. Gossuin, Y.; Hocq, A.; Gillis, P.; Quoc Lam, V. Physics of Magnetic Resonance Imaging: From Spin to Pixel. *J. Phys. D* **2010,** *4*, 213001.
20. Brooks, R. A. T_2-Shortening by Strongly Magnetized Spheres: A Chemical Exchange Model. *Magn. Reson. Med.* **2002,** *47*, 388–391.
21. Li, B.; Ding, D.; Sun, P.; Wang, Y.; Ma, J.; He, B. PGSE NMR Studies of Water States of Hydrogel P(Am-NaA). *J. Appl. Polym. Sci.* **2000,** *77*, 424–427.
22. Penke, B.; Kinsey, S.; Gibbs, S. J.; Moerland, T. S.; Locke, B. R. Proton Diffusion and T_1 Relaxation in Polyacrylamide Gels: A Unified Approach Using Volume Averaging. *J. Magn. Reson.* **1998,** *132*, 240–254.
23. Ray, S. S.; Rajamohanan, P. R.; Badiger, M. V.; Devotta, I.; Ganapathy, S.; Mashelkar, R. A. Self-Diffusion of Water in Thermoreversible Gels Near Volume Transition: Model Development and PFG NMR Investigation. *Chem. Eng. Sci.* **1998,** *53*, 869–877.
24. Gillis, P.; Moiny, F.; Brooks, R. A. On T_2-Shortening by Strongly Magnetized Spheres: A Partial Refocusing Model. *Magn. Reson. Med.* **2002,** *47*, 257–263.
25. Matsumoto, Y.; Jasanoff, A. T_2 Relaxation Induced by Clusters of Superparamagnetic Nanoparticles: Monte Carlo Simulations. *Magn. Reson. Imaging* **2008,** *26*, 994–998.
26. Boxerman, J. L.; Hamberg, L. M.; Rosen, B. R.; Weisskoff, R. M. MR Contrast Due to Intravascular Magnetic Susceptibility Perturbations. *Magn. Reson. Med.* **1995,** *34*, 555–566.
27. Weisskoff, R. M.; Zuo, C. S.; Boxerman, J. L.; Rosen, B. R. Microscopic Susceptibility Variation and Transverse Relaxation: Theory and Experiment. *Magn. Reson. Med.* **1994,** *31*, 601–610.
28. Hardy, P. A.; Henkelman, R. M. Transverse Relaxation Rate Enhancement Caused by Magnetic Particulates. *Magn. Reson. Imaging* **1989,** *7*, 265–275.
29. Berret, J. F.; Schonbeck, N.; Gazeau, F.; El Kharrat, D.; Sandre, O.; Vacher, A.; Airiau, M. Controlled Clustering of Superparamagnetic Nanoparticles Using Block Copolymers: Design of New Contrast Agents for Magnetic Resonance Imaging. *J. Am. Chem. Soc.* **2006,** *128*, 1755–1761.
30. Miyata, T.; Uragami, T.; Nakamae, K. Biomolecule-Sensitive Hydrogels. *Adv. Drug Delivery Rev.* **2002,** *54*, 79–98.
31. Takashi, M.; Asami, N.; Uragami, T. Structural Design of Stimuli-Responsive Bioconjugated Hydrogels That Respond to a Target Antigen. *J. Polym. Sci., Part B* **2009,** *47*, 2144–2157.
32. Bonanno, L. M.; Delouise, U. A. Integration of a Chemical-Responsive Hydrogel into a Porous Silicon Photonic Sensor for Visual Colorimetric Readout. *Adv. Funct. Mater.* **2010,** *20*, 573–578.
33. Wu, D. H.; Chen, A. D.; Johnson, C. S. An Improved Diffusion-Ordered Spectroscopy Experiment Incorporating Bipolar-Gradient Pulses. *J. Magn. Reson., Ser. A* **1995,** *115*, 260–264.